12-2019

The Northwestern Greenland Ice Sheet During The Early Pleistocene Was Similar To Today

Andrew J. Christ
University of Vermont

Paul R. Bierman
University of Vermont

Paul C. Knutz
Geological Survey of Denmark and Greenland

Lee B. Corbett
University of Vermont

Julie C. Fosdick
University of Connecticut

See next page for additional authors

Recommended Citation

Christ, A. J., Bierman, P. R., Knutz, P. C., Corbett, L. B., Fosdick, J. C., Thomas, E. K., et al. (2020). The northwestern Greenland Ice Sheet during the Early Pleistocene was similar to today. Geophysical Research Letters, 47, e2019GL085176. https://doi.org/10.1029/2019GL085176

Geophysical Research Letters

RESEARCH LETTER
10.1029/2019GL085176

The Northwestern Greenland Ice Sheet During The Early Pleistocene Was Similar To Today

Andrew J. Christ[1,2], Paul R. Bierman[1,2], Paul C. Knutz[3], Lee B. Corbett[1], Julie C. Fosdick[4], Elizabeth K. Thomas[5], Owen C. Cowling[5], Alan J. Hidy[6], and Marc W. Caffee[7,8]

[1]Department of Geology, University of Vermont, Burlington, VT, USA, [2]Gund Institute for Environment, University of Vermont, Burlington, VT, USA, [3]Geophysics Department, Geological Survey of Denmark and Greenland, Copenhagen, Denmark, [4]Department of Geosciences, University of Connecticut, Storrs, CT, USA, [5]Department of Geology, State University of New York at Buffalo, Buffalo, NY, USA, [6]Center for Accelerator Mass Spectrometry, Lawrence Livermore National Laboratory, Livermore, CA, USA, [7]Department of Physics and Astronomy, Purdue University, West Lafayette, IN, USA, [8]Department of Earth, Atmospheric, and Planetary Sciences, Purdue University, West Lafayette, IN, USA

Key Points:
- By the Early Pleistocene, the northwestern Greenland Ice Sheet had removed preglacial soil and regolith but had not yet incised deep fjords
- Similar to today, ice-free areas harbored vegetation that was incorporated into glacial marine sediment during ice advances
- Glacial marine diamict is an underutilized, but promising paleoclimate archive; existing archives should be re-examined

Supporting Information:
- Supporting Information S1
- Table S1

Correspondence to:
A. J. Christ,
andrew.christ@uvm.edu

Citation:
Christ, A. J., Bierman, P. R., Knutz, P. C., Corbett, L. B., Fosdick, J. C., Thomas, E. K., et al. (2020). The northwestern Greenland Ice Sheet during the Early Pleistocene was similar to today. *Geophysical Research Letters*, *47*, e2019GL085176. https://doi.org/10.1029/2019GL085176

Received 28 AUG 2019
Accepted 14 DEC 2019
Accepted article online 18 DEC 2019

Abstract The multi-million year history of the Greenland Ice Sheet remains poorly known. Ice-proximal glacial marine diamict provides a direct but discontinuous record of ice sheet behavior; it is underutilized as a climate archive. Here, we present a novel multiproxy analysis of an Early Pleistocene marine diamict from northwestern Greenland. Low cosmogenic nuclide concentrations indicate minimal near-surface exposure, similar to modern terrestrial sediment. Detrital apatite (U-Th-Sm)/He (AHe) ages all predate glaciation by >150 million years, suggesting the northwestern Greenland Ice Sheet had, by 1.9 Ma, not yet incised fjords of sufficient depth to excavate grains with young AHe ages. The diamict contains terrestrial plant leaf wax, likely from land surfaces surrounding the ice sheet. These data indicate that a persistent, dynamic ice sheet existed in northwestern Greenland by 1.9 Ma and that diamict is a useful archive of ice sheet history and process.

Plain Language Summary The behavior of the Greenland Ice Sheet over the past several million years is poorly known. We analyzed 1.9 million-year-old sediment, deposited by glacial ice on the seafloor, to understand long-term ice sheet history. Low cosmogenic isotope concentrations indicate persistent ice cover and at least meters of glacial erosion. Old apatite ages suggest deep glacial valleys had not yet been eroded. Leaf waxes produced by plants and algae indicate less than complete ice cover. By 1.9 million years ago, the Greenland Ice Sheet was a persistent, dynamic, erosive feature of Earth's climate and landscape.

1. Introduction

Understanding Greenland Ice Sheet (GrIS) behavior during warmer-than-present climates is critical (Clark et al., 2016); yet, the behavior and state of the GrIS before the Last Glacial Maximum remain poorly understood (Bierman et al., 2016) because present ice cover obscures and glacial erosion removed terrestrial records of GrIS history (Funder et al., 2001; McFarlin et al., 2018). Much of the known GrIS deep time history relies on marine archives including seismic surveys (Knutz et al., 2019) and sediment cores from deep ocean drilling (Bierman et al., 2016; Helland & Holmes, 1997; Reyes et al., 2014; Tripati et al., 2008) (Figure 1). Deep water cores, generally located far from GrIS outlets, record not only input from Greenland, but also changes in global climate and glaciers on adjacent landmasses. Scarce coarse-grained material in deep-marine sediment limits techniques used in terrestrial environments including cosmogenic nuclides (Dunai, 2010) and low-temperature thermochronometers (Farley, 2002).

Ice-proximal glacial marine deposits are a promising archive of ice sheet change. Repeated ice sheet expansions eroded the Greenland landscape and deposited diamict, a poorly sorted mixture of sediment, accessible by shallow coring, on the continental shelf (Knutz et al., 2019). Relative to deep-marine records, diamict is underutilized as a climate archive because it can be difficult to recover, interpret, and date (Barker et al., 1999). Yet, diamict offers several advantages relative to pelagic sediments. Unlike ice-rafted debris in deep-marine sediments, ice-proximal diamict reduces uncertainty about sediment provenance. Diamict often contains abundant sand-sized grains and a mixture of minerals, allowing for varied analyses.

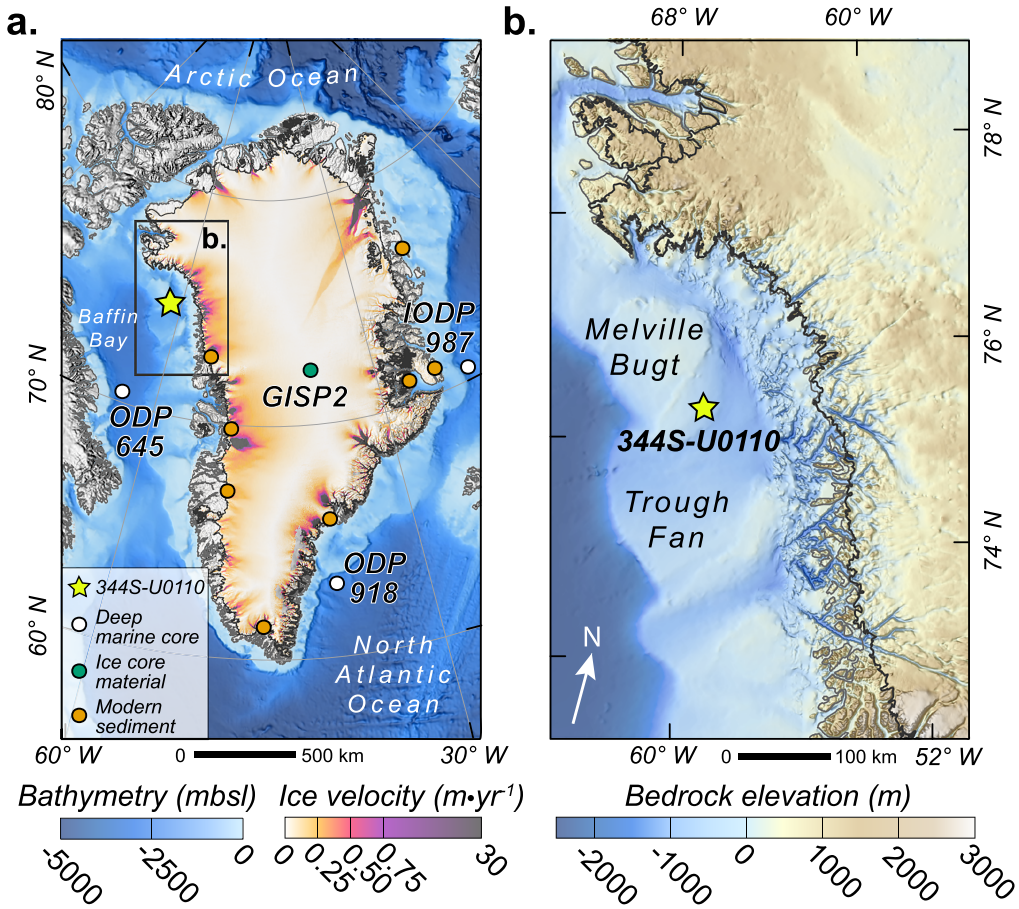

Figure 1. Study area. (a) Greenland and locations of this study (yellow star) and other ^{10}Be studies (circles): marine cores (white) (Bierman et al., 2016; Shakun et al., 2017), bedrock (Schaefer et al., 2016), and basal ice (Bierman et al., 2014) from the GISP2 ice core (green), and modern terrestrial sediment (orange) (Bierman et al., 2014; Corbett, Bierman, Neumann, et al., 2017; Goehring et al., 2010; Graly et al., 2018; Nelson et al., 2014); colors correspond to Figure 2. Elevation data: International Bathymetric Chart of the Arctic Ocean; ice velocity data: ESA Sentinel-1. Coastline (gray) and grounding line (black) also shown. (b) Bedrock topography of northwestern Greenland and Melville Bugt with core 344S-U0110 (yellow star). Elevation data: BedMachine3.

As a proof-of-concept, we examined diamict from Core 344S-U0110 recovered from Melville Bugt (Figure 1). Olduvai paleomagnetic age constraints, combined with well chronologies tied to seismic reflection data, indicate this diamict is Early Pleistocene (1.8–2.0 Ma) (Knutz et al., 2019). These glacial sediments were deposited during the early phase of the Melville Bugt trough-mouth fan, a large paleo–ice sheet drainage system on the northwestern Greenland margin (Figure 1b) (Knutz et al., 2019) (supporting information). Ice cover obscures much of the bedrock geology of northwestern Greenland, which is generally characterized by Archean to Proterozoic crystalline and metasedimentary rocks, Ordovician carbonates, Mesozoic basalts, Cretaceous to Early Cenozoic sedimentary rocks, and extensive Paleogene volcanics (Gregersen et al., 2019). Ice-proximal glacial diamict on the continental shelf in Melville Bay is sourced from these rocks.

We report a novel combination of analyses—meteoric ^{10}Be (^{10}Be$_m$), in situ produced ^{10}Be and ^{26}Al (^{10}Be$_i$, ^{26}Al$_i$), apatite (U-Th-Sm)/He thermochronology (AHe), and lipid biomarkers—on this glacial marine diamict. The abundance of sand-sized material and diversity of minerals allow analyses that are impractical in fine-grained, ice-distal sediment. This multiproxy analysis of glacial diamict delineates the state and behavior of the GrIS during the Early Pleistocene. We present multiple lines of evidence that constrain landscape exposure and erosion histories on different time and depth scales. These data illuminate the similarities and differences between the Early Pleistocene and modern GrIS.

2. Material and Methods

A 70-cm interval was obtained from site 344S-110 that cored a 124 m thick section of muddy diamict (Acton & E.S. Scientists, 2012; Knutz et al., 2019). The sample was from Site U110 in an interval with high recovery (80.20–80.90 m below seafloor) and corresponds with an Early Pleistocene shelf edge ice advance. The sample was separated into different grain sizes (<125, 125–250, 250–850, 850–2,000, >2,000 μm), shapes (angular vs. rounded), and mineral fractions (mafic vs. quartz) (Figure S1). During sieving, we observed small carbonate shell fragments. Approximately 20% of quartz grains were well-rounded and some were iron-stained. These observations suggest the diamict is composed of marine and terrestrial sediments with variable weathering histories. From 1.2 kg of sediment, each size fraction yielded sufficient sample material for cosmogenic nuclide, AHe, and lipid biomarker analyses. Supporting information contains detailed laboratory procedures.

Cosmogenic ^{10}Be and ^{26}Al concentrations in rocks and sediments reveal near-surface landscape exposure, erosion, and burial histories (Dunai, 2010). Meteoric ^{10}Be ($^{10}Be_m$) is produced in the atmosphere and delivered to Earth's surface where it accumulates in soil, regolith, and pelagic sediments (Graly et al., 2010). Elevated $^{10}Be_m$ in glacial marine diamict reflects the erosion and transport of long-exposed soil or regolith from preglacial and/or interglacial landscapes (Graly et al., 2018) and pelagic sedimentation during reduced sea ice cover (Yokoyama et al., 2016). Low $^{10}Be_m$ suggests removal of preglacial regolith and/or substantial sea ice cover. We analyzed $^{10}Be_m$ in grain coatings on all grain size fractions and mineral and shape fractions for grains >125 μm ($n = 9$).

On ice-free landscapes, $^{10}Be_i$ and $^{26}Al_i$ are produced in situ in the upper 2–3 m of near-surface rock and sediment by neutron spallation with minor muonogenic production extending tens of meters (Dunai, 2010). Wet-based glaciers excavate into subsurface material with low $^{10}Be_i$ and $^{26}Al_i$ concentrations, while reexposure during periods with reduced ice cover increases these concentrations in surface materials (Bierman et al., 2016; Shakun, Corbett, Bierman, Underwood, Rizzo, Zimmerman, Caffee, Naish, & Golledge, 2018; Shakun, Corbett, Bierman, Underwood, Rizzo, Zimmerman, Caffee, Naish, Golledge, & Hay, 2018). $^{10}Be_i$ and $^{26}Al_i$ are produced in Greenland at a ratio of 7.3 ± 0.3 in surface materials (Corbett et al., 2017) and higher ratios at depth by muons (Balco, 2017). The half-life of $^{26}Al_i$ is less than $^{10}Be_i$; thus, measured deviations from the production ratio reflect complex exposure, erosion, and/or burial histories. To infer predepositional sediment history, ^{10}Be and ^{26}Al concentrations are decay corrected to the deposition time. We analyzed $^{10}Be_i$ and $^{26}Al_i$ on all quartz fractions >125 μm ($n = 6$), including one duplicate sample (250–850 μm), and shape (angular vs. round) in the 850–2,000 μm fraction.

In glacial settings, low-temperature thermochronometers, including AHe, quantify the timing and magnitude of crustal erosion within sediment source areas, providing constraints on ice sheet incision that excavates glacial valleys and fjords (Christeleit et al., 2017; Ehlers et al., 2015). The AHe thermochronometer relies on production of ^{4}He from radioactive decay of U and Th and thermal diffusion of ^{4}He at low closure temperatures, and thus shallow depths (<3 km) in Earth's crust (Farley, 2000; Reiners & Brandon, 2006). He in apatite is partially retained at temperatures below ~70–90 °C—corresponding to shallow depths (<3 km) in Earth's crust—and completely retained below ~30-40 °C, depending on mineral chemistry and cooling rate (Farley, 2002; Flowers et al., 2009; Shuster et al., 2006). Detrital apatite studies of glacial sediments can detect deep glacial valley/fjord incision that excavated apatite grains with young AHe ages (Bernard et al., 2016; Jess et al., 2018; Tochilin et al., 2012). We analyzed 10 detrital apatite grains to investigate whether deep glacial incision along the NW GrIS had produced young AHe ages.

On formerly glaciated continental shelves, where stratified pelagic sediment is rare, lipid biomarkers in diamict provide the opportunity to assess primary production on and surrounding Greenland through time. Terrestrial flora produce long-chain *n*-alkyl lipids, leaf waxes, whereas marine flora produce short-chain *n*-alkyl lipids and long-chain alkenones (Castaneda & Schouten, 2011; Moros et al., 2016; Sachs et al., 2018). The presence of well-preserved *n*-alkanoic acids indicate contemporaneous plant productivity, as *n*-alkanoic acids are more labile; they are less likely than *n*-alkanes to be preserved in and eroded from surrounding sedimentary rocks (Drenzek et al., 2007). We quantified *n*-alkanoic acids, *n*-alkanes, and alkenones in the <125-μm size fraction to assess terrestrial and marine primary production on northwestern Greenland during the early Pleistocene.

3. Results

3.1. Extremely Low Cosmogenic ^{10}Be and ^{26}Al Concentrations

Cosmogenic ^{10}Be and ^{26}Al concentrations, decay corrected for 1.9 Ma of postdepositional burial, are extremely low across all sediment sizes, shapes, and mineral fractions, with $^{10}Be_m$ (10^5–10^7 atoms g^{-1}) at least 2 orders of magnitude greater than $^{10}Be_i$ (10^3 atoms·g^{-1}) (Figure 2 and Tables S1 and S2). Neither $^{10}Be_m$ nor $^{10}Be_i$ concentrations are related to grain size, except the fine fraction (GEUS01: <125 um), which had the highest decay-corrected $^{10}Be_m$ concentration ($4.1 \pm 0.01 \times 10^7$ atoms g^{-1}; weighted mean ±1 sigma) (Table S1 and Figure 2). Decay-corrected $^{10}Be_m$ adhering to mafic minerals ($1.7 \pm 0.6 \times 10^6$ atoms g^{-1}, $n = 3$) was an order of magnitude greater than quartz fractions ($3.8 \pm 0.1 \times 10^5$ atoms g^{-1}, $n = 5$). Mass-weighted-mean decay-corrected concentrations of $^{10}Be_i$ ($5.3 \pm 2.0 \times 10^3$ atoms·g^{-1}) and $^{26}Al_i$ ($4.8 \pm 2.3 \times 10^4$ atoms·g^{-1}) were low ($n = 6$), displayed no grain size trend, and yield a weighted-mean $^{26}Al_i/^{10}Be_i$ ratio of 9.1 ± 1.5 (Figure S4 and Tables S2, S4, and S6).

3.2. Old (>160 Ma) Detrital AHe Ages

Detrital apatite yielded single-grain AHe ages from 159 to 686 Ma (Figures 3 and S5 and Table S7) with no Cenozoic ages. The 10 AHe ages fall into four groups (Figure 3): Jurassic (159–181 Ma, $n = 3$), Late Triassic (221–228 Ma, $n = 2$), Late Carboniferous-Permian (267–305 Ma, $n = 4$), and Neoproterozoic (686 Ma, $n = 1$), with no apparent correlations between age and grain size (~70–82 μm) (Figure S5a) or Th/U (0.03–1.6) (Figure S5c). Effective uranium concentrations (eU), a proxy for natural radiation damage to crystal lattices, range from ~2 to 78 ppm (Figure S3b). A negative correlation between age and eU suggests some radiation damage influence on He diffusion, and thus closure temperature and AHe ages (Flowers et al., 2009). For apatite with this range of eU (using a radiation diffusion model after Flowers et al., 2009, and 1 °C/Ma monotonic cooling rate), we estimate closure temperatures of ~45–70 °C. Corresponding closure depths of ~1.3–3.0 km (assuming 20–28 °C/km crustal geotherm, Martos et al., 2018, and 10 °C average surface temperature) provide an upper limit on erosion depth within the sediment source areas.

3.3. Well-Preserved Lipid Biomarkers

The diamict contains well-preserved lipid biomarkers (Figure 4). Alkenones are present in the sediment, but at low concentration (<50 ng·g^{-1} dry sediment, $C_{37:2}$ and $C_{37:3}$ combined). Short-chain *n*-alkanoic acids are most abundant (C_{16}: 990 ± 152 ng·g^{-1}, C_{18}: 1449 ± 197 ng·g^{-1}; Figure 4a and Table S8), while middle- and long-chain *n*-alkanoic acids are present at lower concentrations: C_{28} is most abundant, 482 ± 96 ng·g^{-1} (Table S8). The *n*-alkanoic acids have a strong even-over-odd preference (4.3 ± 0.6), indicating minimal degradation, as plant biosynthesis produces even-chain *n*-alkanoic acids (Eglinton & Eglinton, 2008). The *n*-alkane concentrations are lower than *n*-alkanoic acids (C_{29} is most abundant [309 ± 33 ng·g^{-1}]; Figure 4b and Table S8), with a lower odd-over-even preference (2.4 ± 0.1), indicating potential contamination by organic matter from sedimentary rocks.

4. Discussion

4.1. Glacial Erosion of Pre–ice Sheet Regolith by the Early Pleistocene

Low $^{10}Be_m$, $^{10}Be_i$, and $^{26}Al_i$ in this shelf diamict—for all grain sizes, shapes, or mineralogies—suggest the northwestern GrIS eroded at least several meters of surficial material from sediment source areas by the Early Pleistocene. Low cosmogenic nuclide concentrations mandate only minimal contribution from sediment exposed at or near Earth's surface. Even grains with apparent surface weathering characteristics, including rounded, iron-stained sand (GEUS06), yield low $^{10}Be_i$ concentrations ($1.7 \pm 2.0 \times 10^3$ atoms·g^{-1}) suggesting a long-buried origin, possibly from erosion of nearby Cretaceous sandstones (Gregersen et al., 2019).

This early Pleistocene diamict is sourced from an area with minimal exposure and high erosion rates, and thus comprised of deeply eroded materials. The 1.9 Ma decay-corrected $^{26}Al_i/^{10}Be_i$ ratio of this diamict (9.1 ± 1.5; weighted mean ± 1 sigma), while variable, is greater than the contemporary Greenland surface production ratio of 7.3 ± 0.3 (Corbett, Bierman, Rood, et al., 2017) (Table S6 and Figure S4). $^{26}Al_i/^{10}Be_i$ ratios >7 are indicative of muon-induced production at depths of tens of meters for short (~100 kyr) periods (Balco, 2017). Low nuclide concentrations, yet high a $^{26}Al_i/^{10}Be_i$ ratio, are consistent with erosion of several meters

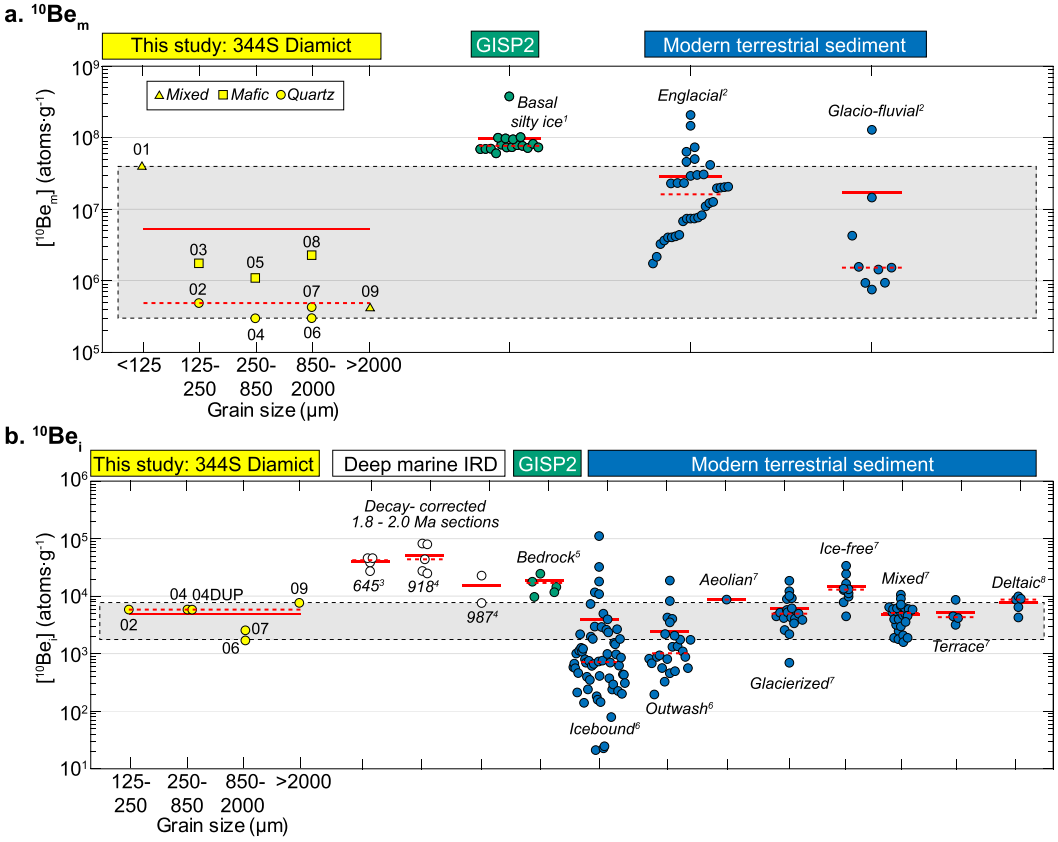

Figure 2. Cosmogenic (a) $^{10}Be_m$ and (b) $^{10}Be_i$ concentrations in sediments from this study (yellow) and other Greenland archives: deep-marine IRD (white), GISP 2 ice core basal material (green), and modern terrestrial sediment (blue). ^{10}Be concentrations in diamict (this study) are decay corrected for 1.9 Ma burial time and presented by grain size and mineral fraction. Samples labeled with numerical suffix (i.e., GEUS 01). Error bars are less than the symbol size. Red lines show mean (solid) and median (dashed) for all data sets. Gray box outlines the range of ^{10}Be measurements from this study for comparison. Superscripts correspond to 1 = Bierman et al. (2016); 2 = Graly et al. (2018); 3 = Shakun, Corbett, Bierman, Underwood, Rizzo, Zimmerman, Caffee, Naish, and Golledge (2018), Shakun, Corbett, Bierman, Underwood, Rizzo, Zimmerman, Caffee, Naish, Golledge, and Hay (2018); 4 = Bierman et al. (2014); 5 = Schaefer et al. (2016); 6 = Corbett, Bierman, Neumann, et al. (2017); 7 = Nelson et al. (2014); 8 = Goehring et al. (2010).

of surface material prior to 2.0 Ma (which would have higher $^{10}Be_i$ and $^{26}Al_i$ concentrations and a lower $^{26}Al_i/^{10}Be_i$) followed by brief exposure at depth, then erosion and subglacial transport to the shelf margin. Such early glacial erosion followed by exposure fits with ice-free conditions indicated by the ~2 Ma Kap København Formation that putatively predates the diamict we analyzed (Funder et al., 2001). The presence

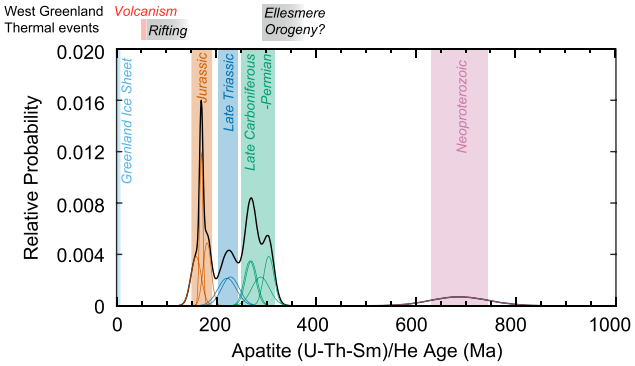

Figure 3. Probability density function of (U-Th-Sm)/He ages of detrital apatites. Thin lines: individual Gaussian age distributions color coded by age grouping; thick line: population (n = 10) cumulative probability density function. Text above refers to thermal-tectonic events in West Greenland (Alsulami et al., 2015; Gregersen et al., 2019; Henriksen et al., 2009).

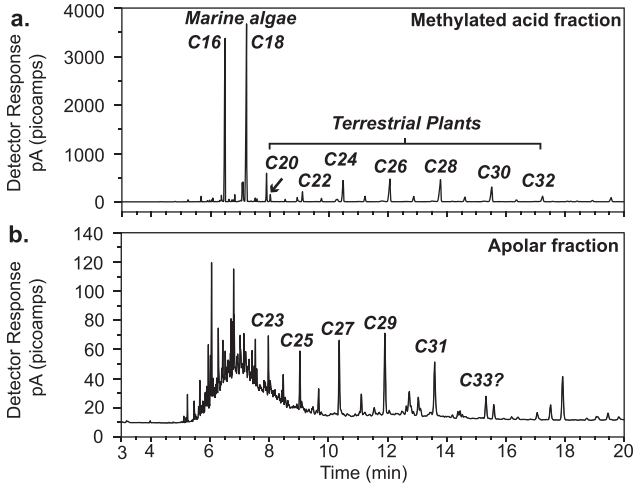

Figure 4. Lipid biomarker results. (a) Methylated acid fraction, even-chain length fatty acid methyl ester peaks labeled with carbon chain number. (b) Apolar fraction, odd-chain length *n*-alkane peaks labeled with carbon chain number.

of $^{26}Al_i$ supports the age model (Knutz et al., 2019); if the diamict was much older than 2.0 Ma, $^{26}Al_i$ would not be preserved due to its 7×10^5 year half-life.

Decay-corrected $^{10}Be_i$ concentrations in diamict (10^3 atoms·g^{-1}; this study) are an order of magnitude less than in ice-rafted debris (10^4 atoms·g^{-1}) in sections of similar age in deep-marine cores surrounding Greenland (Bierman et al., 2016). Thus, this glacial marine sediment on the northwestern Greenland shelf has a different exposure and erosional history than ice-rafted debris of similar age recovered in deep-marine cores (Figure 2) (Bierman et al., 2016; Shakun, Corbett, Bierman, Underwood, Rizzo, Zimmerman, Caffee, Naish, & Golledge, 2018; Shakun, Corbett, Bierman, Underwood, Rizzo, Zimmerman, Caffee, Naish, Golledge, & Hay, 2018). Elevated decay-corrected $^{10}Be_i$ concentrations in ice-rafted debris could result from subaerially exposed sediment sources, including regolith predating glaciation or rockfall from exposed highlands.

Different $^{10}Be_m$ and $^{10}Be_i$ concentrations in shelf diamict and GrIS basal material (Bierman et al., 2014; Bierman et al., 2016; Graly et al., 2018; Schaefer et al., 2016) highlights how spatially heterogeneous ice sheet basal thermal regimes controlled GrIS erosion since the Early Pleistocene, similar to other ice sheets (Gjermundsen et al., 2015). Concentrations of $^{10}Be_m$ in silt from basal ice (10^7–10^8 atoms·g^{-1}) (Bierman et al., 2016) and $^{10}Be_i$ in subglacial bedrock (10^4 atoms·g^{-1}) (Schaefer et al., 2016) at the base of the GISP2 ice core are at least an order of magnitude greater than decay-corrected $^{10}Be_m$ (10^5-10^6 atoms·g^{-1}) and $^{10}Be_i$ (10^3 atoms·g^{-1}) concentrations in this diamict (Figure 2). This suggests a polythermal GrIS where cold-based sectors preserve old soils and previously exposed bedrock surfaces. In contrast, where the base of the GrIS reaches pressure melting, ice excavates into the underlying rock where little $^{10}Be_m$ and $^{10}Be_i$ accumulated. Even if some sediment is sourced from surfaces with high $^{10}Be_i$ or $^{26}Al_i$ concentrations, cosmogenic nuclide concentrations in offshore diamict must be diluted by a large contribution of sediment from deeply eroded areas.

The Early Pleistocene shelf diamict we analyzed isotopically resembles sediment discharged at the ice sheet margin today (Graly et al., 2018; Nelson et al., 2014) (Fig. 2). $^{10}Be_m$ concentrations (10^5–10^7 atoms·g^{-1}) are similar to $^{10}Be_m$ measurements in modern englacial sediment (10^6–10^8 atoms·g^{-1}) and subglacial and glaciofluvial sediment (10^5–10^7 atoms·g^{-1}) from the edge of the GrIS (Graly et al., 2018). $^{10}Be_i$ concentrations (10^3 atoms·g^{-1}) more closely resemble those in modern terrestrial sediment from glacierized regions (10^3–10^4 atoms·g^{-1}) than ice-free areas (10^4–10^5 atoms·g^{-1}) (Goehring et al., 2010; Nelson et al., 2014; Corbett, Bierman, Neumann, et al., 2017). We infer that Early Pleistocene GrIS erosional processes were similar to today with zones of erosive ice that produce sediments with low $^{10}Be_i$ concentrations, while cold-based sectors preserve higher $^{10}Be_i$ concentrations.

4.2. The Absence of Deeply Carved Fjords in Melville Bugt

While cosmogenic nuclide data imply source erosion of at least several meters, consistently old (>160 Ma) AHe ages do not provide evidence for fjord-scale glacial incision (>1.3 km) by 2.0 Ma (Figure 3). Apatites with Late Carboniferous-Permian AHe ages may correspond to sediment sources from the Ellesmerian Orogenic belt in northernmost Greenland (Henriksen et al., 2009). The timing of deformation from this event is not well known, but postdated the late Devonian (370 Ma). Apatites of Jurassic age predate Cretaceous rifting and Paleogene basalt volcanism (Alsulami et al., 2015) in West Greenland; there are no known sources or thermogenic events that can explain these grain ages (Gregersen et al., 2019).

The lack of AHe ages <150 Ma suggests that the diamict was sourced from areas that underwent little Pliocene or Early Pleistocene incision, although a large-*n* detrital analysis is necessary to resolve potential source areas. Sediment derived from deep erosion of fjords would yield AHe ages younger than known thermal events, similar to northeast Greenland (Bernard et al., 2016) or the Patagonian Ice Sheet incision of the Andes (Christeleit et al., 2017). Such sediment sources may include the higher topographic levels of present day fjords and intervening ridges, and/or the low-relief plateau areas within the Greenland continental

margin (Figure 1b). While our cosmogenic nuclide data indicate stripping of the preglacial or interglacial landscape, consistently old AHe ages indicate that glacial erosion beneath the NW GrIS had not incised fjord-scale features by 1.9 Ma.

4.3. Early Pleistocene Terrestrial Primary Productivity on Greenland

Despite evidence for meters of glacial erosion, biomarkers recovered from the diamict indicate sediment input from regions with terrestrial vegetation (Figure 4); this requires ice-free conditions around the ice sheet margins prior to 1.8–2.0 Ma. Holocene terrestrial plants and lake sediments on Greenland do not contain high concentrations of short chain ($<C_{20}$) *n*-alkanoic acids or *n*-alkanes but do contain abundant middle- and long-chain *n*-alkanoic acids and *n*-alkanes, up to 2 orders of magnitude more concentrated than in the diamict we analyzed (Berke et al., 2019; Thomas et al., 2016; Thomas et al., 2018). The diamict is dominated by longer chain length *n*-alkanoic acids (C_{26} and C_{28}) than in Greenland Holocene lake sediments, which have additional input from aquatic macrophytes and are dominated by C_{24} (Thomas et al., 2016). We infer the C_{20} to C_{32} *n*-alkanoic acids are derived from terrestrial plants growing in exposed areas around the GrIS margin, similar to the Holocene. Strong even-over-odd preference of *n*-alkanoic acids indicates these compounds are well preserved and likely were not subaerially exposed for long before deposition in this diamict. Given the concentration and preservation of these biomarkers, it is unlikely that they are derived from windblown material. The preservation of long-chain *n*-alkanoic acids in this diamict indicates that vegetation-covered ice-free areas of northwestern Greenland before transport by later ice sheet advance(s) and deposition in this diamict.

The presence of marine algal lipids, shell fragments, and elevated $^{10}Be_m$ in the <125 μm fraction (GEUS01) suggest grounded ice reworked marine sediments from earlier periods of reduced ice cover on the shelf (Figure 4). Short-chain *n*-alkanoic acids, produced by marine algae throughout the Arctic Ocean today (Sachs et al., 2018), and alkenones—biomarkers of marine coccolithophores (Moros et al., 2016)—indicate marine sediment sources (Sachs et al., 2018). Higher $^{10}Be_m$ concentrations in GEUS01 < 125 μm ($41.0 \pm 0.001 \times 10^6$ atoms·g^{-1}), relative to all other measurements on fractions >125 μm (average: $0.89 \pm 0.71 \times 10^6$ atoms·g^{-1}) suggest the fine fraction is a mixture of pelagic and subglacially derived sediment. In modern glacial marine environments like the Ross Sea, Antarctica, the transition from sub–ice shelf to open marine conditions during the Holocene increased $^{10}Be_m$ concentrations in sediment (up to 10^9 atoms·g^{-1}) (Yokoyama et al., 2016). Yet, decay-corrected concentrations in 344S diamict are 2 orders of magnitude lower than Holocene measurements in the Ross Sea. Elevated $^{10}Be_m$ in the fine sediment fraction of Early Pleistocene 344S diamict likely reflects a mixture of reworked pelagic sediments ($^{10}Be_m$-rich) and subglacially derived ($^{10}Be_m$-poor) fine sediment.

5. Implications

Our data suggest that during the Early Pleistocene, northwestern Greenland was similar to today with substantial ice cover, glacial erosion below warm-based ice, and coastal ice-free areas that harbored vegetation. These data suggest the presence of a largely persistent, yet dynamic, ice sheet in northwestern Greenland by the Early Pleistocene (Knutz et al., 2019). Decay-corrected ^{10}Be concentrations in diamict resemble ^{10}Be measurements of sediment discharged from the GrIS today (Figure 2) and the decay-corrected $^{26}Al_i/^{10}Be_i$ ratio, while uncertain, exceeds the observed Greenland surface production ratio (Corbett, Bierman, Rood, et al., 2017). These observations suggest that most subglacial material we analyzed was sourced from regions with high erosion rates. Sediment discharged to the ice margin effectively diluted sediment from ice-free areas (Nelson et al., 2014). By 1.9 Ma, subglacial erosion in northwestern Greenland already removed surface materials, leaving only a few thousand atoms·g^{-1} of $^{10}Be_i$ and $^{26}Al_i$ in quartz grains, most likely produced by muon reactions at tens of meters depth.

Ice-free conditions in source areas of the diamict were so limited—either spatially or temporally—that ^{10}Be could not accumulate significantly in rocks or sediment before glacial erosion. Low cosmogenic nuclide concentrations in marine diamict versus elevated concentrations in GISP2 subglacial bedrock highlights the polythermal conditions, and therefore varied erosional efficiency, beneath GrIS. In contrast, old detrital AHe ages indicate that glacial denudation of sediment source areas, while sufficient to remove most $^{10}Be_i$ and $^{26}Al_i$, had not carved deep fjords before 1.9 Ma in northwestern Greenland. Abundant well-preserved

terrestrial and marine lipid biomarkers, bivalve fragments, and elevated $^{10}Be_m$ in <125 μm sediment suggest the ice sheet transported and reworked sediments originally deposited under both open-marine conditions and from ice-free marginal areas.

Multiparameter analyses of glacial diamict demonstrate its utility as an archive of glacial processes in presently deglaciated margins. Systematic analysis of glacial diamict will allow assessment of long-term changes in glacial erosion, ice cover, and vegetation throughout polar regions. Because diamict is a mixture of eroded sediment, it integrates and contains information about surface processes. Lipid biomarkers provide insight into ecosystems whereas cosmogenic nuclides and detrital apatite (U-Th-Sm)/He ages in diamict provide information about erosion to different depths. Diamict offers a promising archive of climate and ice sheet history.

Acknowledgments
Study inspired by a MagellanPlus workshop at GEUS supported by ECORD (PKN). We thank K. Hollister (Buffalo) and A. Goldsmith, Connecticut Basin Analysis and Thermochronology Laboratory (EAR-1735492 to J. C. F.); Colorado TRaIL for U and Th determinations; Vermont Community Cosmogenic Facility (EAR-1735676 to P. R. B.); M. Quock for mineral picking. Prepared by LLNL under Contract DE-AC52-07NA27344; LLNL-JRNL-774748. PRIME Lab (EAR-1560658). Authors declare no conflicts of interest. All data available in the supporting information and Open Science Framework (https://osf.io/3g6a2/, DOI: https://10.17605/OSF.IO/3G6A2).

References

Acton, G., & E. S. Scientists (2012). Expedition 344S Rep., 844 pp, International Ocean Discovery Program.
Alsulami, S., Paton, D. A., & Cornwell, D. G. (2015). Tectonic variation and structural evolution of the West Greenland continental margin. *AAPG Bulletin*, *99*(9), 1689–1711.
Balco, G. (2017). Production rate calculations for cosmic-ray-muon-produced 10Be and ^{26}Al benchmarked against geological calibration data. *Quaternary Geochronology*, *39*, 150–173.
Barker, P. F., Camerlenghi, A., Acton, G. D., & S. S. Party (1999). Leg 178 Summary*Rep*., 174 pp.
Berke, M. A., Cartagena Sierra, A., Bush, R., Cheah, D., & O'Connor, K. (2019). Controls on leaf wax fractionation and δ^2H values in tundra vascular plants from western Greenland. *Geochimica et Cosmochimica Acta*, *244*, 565–583.
Bernard, T., Steer, P., Gallagher, K., Szulc, A., Whitman, A., & Johnson, C. (2016). Evidence for Eocene-Oligocene glaciation in the lanscape of the East Greenland margin. *Geology*, *44*(11), 895–898.
Bierman, P. R., Corbett, L. B., Graly, J. A., Neumann, T. A., Lini, A., Crosby, B. T., & Rood, D. H. (2014). Preservation of a preglacial landscape under the center of the Greenland Ice Sheet. *Science*, *344*(6182), 402–405.
Bierman, P. R., Shakun, J. D., Corbett, L. B., Zimmerman, S. R., & Rood, D. H. (2016). A persistent and dynamic East Greenland Ice Sheet over the past 7.5 million years. *Nature*, *540*(7632), 256–260. https://doi.org/10.1038/nature20147
Castaneda, I. S., & Schouten, S. (2011). A review of molecular organic proxies for examining modern and ancient lacustrine environments. *Quaternary Science Reviews*, *30*, 2851–2891.
Christeleit, E. C., Brandon, M. T., & Shuster, D. L. (2017). Miocene development of alpine glacial relief in the Patagonian Andes, as revealed by low-temperature thermochronometry. *Earth and Planetary Science Letters*, *460*, 152–163.
Clark, P. U., Shakun, J. D., Marcott, S. A., Mix, A. C., Eby, M., Kulp, S., et al. (2016). Consequences of twenty-first-century policy for multi-millennial climate and sea-level change. *Nature Climate Change*, *6*(4), 360–369. https://doi.org/10.1038/nclimate2923
Corbett, L. B., Bierman, P. R., Neumann, T. A., Graly, J. G., Shakun, J. D., Marc, W., et al. (2017). Analysis of three cosmogenic isotopes in subglacial cobbles helps unravel Greenland's exposure and erosion history. GSA Abstracts with Programs, Annual Meeting, Seattle, WA. v. 49(6),Abstract 51-3. https://doi.org/10.1130/abs/2017AM-302307.
Corbett, L. B., Bierman, P. R., Rood, D. H., Caffee, M. W., Lifton, N. A., & Woodruff, T. E. (2017). Cosmogenic $^{26}Al/^{10}Be$ surface production ratio in Greenland. *Geophysical Research Letters*, *44*, 1350–1359. https://doi.org/10.1002/2016GL071276
Drenzek, N. J., Montlucon, D. B., Yunker, M. B., Macdonald, R. W., & Eglinton, T. I. (2007). Constraints on the origin of sedimentary organic carbon in the Beaufort Sea from coupled molecular ^{13}C and ^{14}C measurements. *Marine Chemistry*, *103*(1-2), 146–162.
Dunai, T. J. (2010). *Cosmogenic nuclides: Principles, concepts and applications in the Earth Surface Sciences*. Cambridge: Cambridge University Press.
Eglinton, T. I., & Eglinton, G. (2008). Molecular proxies for paleoclimatology. *Earth and Planetary Science Letters*, *275*(1-2), 1–16.
Ehlers, T. A., Szameitat, A., Enkelmann, E., Yanites, B. J., & Woodsworth, G. J. (2015). Identifying spatial variations in glacial catchment erosion with detrital thermochronology. *Journal of Geophysical Research: Earth Surface*, *120*, 1023–1039. https://doi.org/10.1002/2014JF003432
Farley, K. A. (2000). Helium diffusion from apatite: General behavior as illustrated by Durango fluorapatite. *Journal of Geophysical Research*, *105*(B2), 2903–2914.
Farley, K. A. (2002). (U-Th)/He dating: Techniques, calibrations, and applications. *Noble Gases in Geochemistry and Cosmochemistry*, *47*, 819–844.
Flowers, R. M., Ketcham, R. A., Shuster, D. L., & Farley, K. A. (2009). Apatite (U–Th)/He thermochronometry using a radiation damage accumulation and annealing model. *Geochimica et Cosmochimica Acta*, *73*(8), 2347–2365.
Funder, S., Bennike, O., Bocher, J., Israelson, C., Petersen, K. S., & Simonarson, L. A. (2001). Late Pliocene Greenland—The Kap Kobenhavn Formation in North Greenland. *Bulletin of the Geological Society of Denmark*, *48*, 117–134.
Gjermundsen, E. F., Briner, J. P., Akçar, N., Foros, J., Kubik, P. W., Salvigsen, O., & Hormes, A. (2015). Minimal erosion of Arctic alpine topography during late Quaternary glaciation. *Nature Geoscience*, *8*, 789–792.
Goehring, B. M., Kelly, M. A., Schaefer, J. M., Finkel, R. C., & Lowell, T. V. (2010). Dating of raised marine and lacustrine deposits in east Greenland using beryllium-10 depth profiles and implications for estimates of subglacial erosion. *Journal of Quaternary Science*, *25*(6), 865–874.
Graly, J. A., Bierman, P. R., Reusser, L. J., & Pavich, M. J. (2010). Meteoric ^{10}Be in soil profiles - A global meta-analysis. *Geochimica et Cosmochimica Acta*, *74*(23), 6814–6829.
Graly, J. A., Corbett, L. B., Bierman, P. R., Lini, A., & Neumann, T. A. (2018). Meteoric ^{10}Be as a tracer of subglacial processes and interglacial surface exposure in Greenland. *Quaternary Science Reviews*, *191*, 118–131.
Gregersen, U., Knutz, P. C., Nohr-Hansen, H., Sheldon, E., & Hopper, J. R. (2019). Tectonostratigraphy and evolution of the West Greenland continental margin. *Bulletin of the Geological Society of Denmark*, *67*, 1–21.
Helland, P. E., & Holmes, M. A. (1997). Surface textural analysis of quartz sand grains from ODP Site 918 off the southeast coast of Greenland suggests glaciation of southern Greenland at 11 Ma. *Palaeogeography Palaeoclimatology Palaeoecology*, *135*(1-4), 109–121.
Henriksen, N., Higgins, A. K., Kalsbeek, F., & Pulvertaft, C. R. (2009). Greenland from Archaean to Quaternary descriptive text to the 1995 Geological map of Greenland, 1:2,500,000., *Geological Survey of Denmark and Greenland Bulletin*, *18*, 126.

Jess, S., Stephenson, R., & Brown, R. (2018). Evolution of the central West Greenland margin and the Nuussuaq Basin: Localised basin uplift along a stable continental margin proposed from thermochronological data. *Basin Research*, *30*(6), 1230–1246.

Knutz, P. C., Newton, A. M. W., Hopper, J. R., Huuse, M., Gregersen, U., Sheldon, E., & Dybkjær, K. (2019). Eleven phases of Greenland Ice Sheet shelf-edge advance over the past 2.7 million years. *Nature Geoscience*, *12*, 361–368.

Martos, Y. M., Jordan, T. A., Catalan, M., Jordan, T. M., Bamber, J. L., & Vaughan, D. G. (2018). Geothermal heat flux reveals the Iceland hotspot track underneath Greenland. *Geophysical Research Letters*, *45*, 8214–8222. https://doi.org/10.1029/2018GL078289

McFarlin, J. M., Axford, Y., Osburn, M. R., Kelly, M. A., Osterberg, E. C., & Farnsworth, L. B. (2018). Pronounced summer warming in northwest Greenland during the Holocene and Last Interglacial. *Proceedings of the National Academy of Sciences of the United States of America*, *115*(25), 6357–6362.

Moros, M., Lloyd, J. M., Perner, K., Krawczyk, D., Blanz, T., de Vernal, A., et al. (2016). Surface and sub-surface multi-proxy reconstruction of middle to late Holocene palaeoceanographic changes in Disko Bugt, West Greenland. *Quaternary Science Reviews*, *132*, 146–160. https://doi.org/10.1016/j.quascirev.2015.11.017

Nelson, A. H., Bierman, P. R., Shakun, J. D., & Rood, D. H. (2014). Using *in situ* cosmogenic 10Be to identify the source of sediment leaving Greenland. *Earth Surface Processes and Landforms*, *39*(8), 1087–1100.

Reiners, P. W., & Brandon, M. T. (2006). Using thermochronology to understand orogenic erosion. *Annual Review of Earth and Planetary Sciences*, *34*, 419–466.

Reyes, A. V., Carlson, A. E., Beard, B. L., Hatfield, R. G., Stoner, J. S., Winsor, K., et al. (2014). South Greenland ice-sheet collapse during Marine Isotope Stage 11. *Nature*, *510*(7506), 525–528.

Sachs, J. P., Stein, R., Maloney, A. E., Wolhowe, M., Fahl, K., & Nam, S. I. (2018). An Arctic Ocean paleosalinity proxy from delta H-2 of palmitic acid provides evidence for deglacial Mackenzie River flood events. *Quaternary Science Reviews*, *198*, 76–90. https://doi.org/10.1016/j.quascirev.2018.08.025

Schaefer, J. M., Finkel, R. C., Balco, G., Alley, R. B., Caffee, M. W., Briner, J. P., et al. (2016). Greenland was nearly ice-free for extended periods during the Pleistocene. *Nature*, *540*(7632), 252–255. https://doi.org/10.1038/nature20146

Shakun, J., Corbett, L., Bierman, P., & Zimmerman, S. (2017). Pliocene Greenland ice sheet growth recorded by *in situ* ^{10}Be decrease in multiple marine sediment, paper presented at GSA Abstracts with Programs, Seattle, WA.

Shakun, J. D., Corbett, L. B., Bierman, P. R., Underwood, K., Rizzo, D. M, Zimmerman, S. R., et al. (2018). Eight million years of polar ice sheet variations from cosmogenic nuclides in marine sediments, in *Goldschmidt Conference*, edited, Boston, MA.

Shakun, J. D., Corbett, L. B., Bierman, P. R., Underwood, K., Rizzo, D. M., Zimmerman, S. R., et al. (2018). Minimal East Antarctic Ice Sheet retreat onto land during the past eight million years. *Nature*, *558*(7709), 284–287.

Shuster, D. L., Flowers, R. M., & Farley, K. A. (2006). The influence of natural radiation damage on helium diffusion kinetics in apatite. *Earth and Planetary Science Letters*, *249*, 148–161.

Thomas, E. K., Briner, J. P., Ryan-Henry, J. J., & Huang, Y. (2016). A major increase in winter snowfall during the middle Holocene on western Greenland caused by reduced sea ice in Baffin Bay and the Labrador Sea. *Geophysical Research Letters*, *43*, 5302–5308. https://doi.org/10.1002/2016GL068513

Thomas, E. K., Castaneda, I. S., McKay, N. P., Briner, J. P., Salacup, J. M., Nguyen, K. Q., & Schweinsberg, A. D. (2018). A Wetter Arctic coincident with hemispheric warming 8,000 Years ago. *Geophysical Research Letters*, *45*, 10,637–10,647. https://doi.org/10.1029/2018GL079517

Tochilin, C. J., Reiners, P. W., Thomson, S. N., Gehrels, G. E., Hemming, S. R., & Pierce, E. L. (2012). Erosional history of the Prydz Bay sector of East Antarctica from detrital apatite and zircon geo- and thermochronology multidating. *Geochemistry, Geophysics, Geosystems*, *13*, Q11015. https://doi.org/10.1029/2012GC004364

Tripati, A. K., Eagle, R. A., Morton, A., Dowdeswell, J. A., Atkinson, K. L., Bahé, Y., et al. (2008). Evidence for glaciation in the Northern Hemisphere back to 44 Ma from ice-rafted debris in the Greenland Sea. *Earth and Planetary Science Letters*, *265*(1-2), 112–122. https://doi.org/10.1016/j.epsl.2007.09.045

Yokoyama, Y., Anderson, J. B., Yamane, M., Simkins, L. M., Miyairi, Y., Yamazaki, T., et al. (2016). Widespread collapse of the Ross Ice Shelf during the late Holocene. *Proceedings of the National Academy of Sciences of the United States of America*, *113*(9), 2354–2359. https://doi.org/10.1073/pnas.1516908113